PERGAMON

International Journal of Multiphase Flow 28 (2002) 301–324

International Journal of Multiphase Flow

www.elsevier.com/locate/ijmulflow

Particle concentration and local mass flux measurements in two-phase flows with PDA. Application to a study on the dispersion of spherical particles in a turbulent air jet

L. Aísa, J.A. Garcia *, L.M. Cerecedo, I. García Palacín, E. Calvo

Fluid Mechanics Group, Universidad de Zaragoza, C/Maria de Luna 3, 50015, Zaragoza, Spain

Received 5 October 2000; received in revised form 1 October 2001

Abstract

The Phase Doppler Anemometry (PDA) technique is suitable for spherical particle concentration and local flux measurements in dispersed two-phase flows. When particles have three-directional paths, accurate measurements can be achieved if an integral method of calculation over the effective probe volume and an efficient auto-calibration process are employed. An experimental study is carried out on an axisymmetric two-phase jet. A post-processing of the measurements has been developed to obtain a quite complete characterisation of the particle dispersion throughout the flow. The axial local flux distribution is normalised on the transversal sections with the injected mass rate for each particle size class (by means of correction coefficients). Particle concentration and radial fluxes are calculated from the axial flux and velocity results. A balance of particles over a cylindrical volume permits to calculate further estimates of the particle radial flux, used for testing of the results. The detailed study of the spatial distribution of particles has been made up to 10 nozzle diameters ($10D$) from the jet exit, in five transversal sections. The local axial flux profiles show two development sub-zones: (i) the near to nozzle zone is dominated by the exit conditions. Mainly, a wide distribution of particle path directions produces a strong radial particle transference (directional classification); (ii) the second sub-zone shows a more regular development controlled by the drag of the mean gas velocity field together with radial particle transport by gas turbulence, rebounding crashes of particles and other effects.

Keywords: Particles; Two-phase flows; Concentration and flux PDA measurements; Particle-laden jet

1. Introduction

There is an increasing interest in the detailed measurements of the particle spatial distribution in industrial two-phase flows (e.g. combustion, powder production). In fact, the physical fields

* Corresponding author.

0301-9322/02/$ - see front matter
PII: S0301-9322(01)00071-4

that describe the particle distribution along the flow (e.g. mean particle concentration and mean flux) are some of the most important quantities of the multiphase problems.

Since the beginning, Phase Doppler Anemometry (PDA) has been considered as a useful technique for the concentration and flux measurements of spherical particles (Durst and Umhauer, 1975; Saffman et al., 1984). Several elements are necessary to obtain reliable results. These are:

(i) Accurate measurements of particle parameters (as velocity, diameter, transit time, etc.).
(ii) Suitable algorithms for flux and concentration calculation as well as auto-calibration techniques of probe volume geometry.
(iii) Correction techniques for errors caused by an inaccurate validation of the particle signal. Multiple effects (burst splitting, multiparticle signals, low SNR and so on) cause this variation of the signal number.

The reliable measurement of particle parameters is the subject of numerous basic works about the technique and, therefore, this topic is not analysed in this paper.

Concentration and particle flux calculations need either the number of particles that cross the effective cross-section of the probe volume or other equivalent procedures (e.g. the so-called integral methods). As well as the calculations, probe volume size must be calibrated for each measurement point. A few fundamental studies have been devoted to this subject (Saffman, 1987; Qiu and Sommerfeld, 1992; Zhu et al., 1993; Sommerfeld, 1997).

Sometimes, the quasi one-directional particle movement hypothesis is used to simplify the calculation and calibration procedure. This approximation leads to significant errors when particle paths deviate from the direction of the velocity component measured by the PDA (García, 2000). We have called this effect the directional bias. So, only the methods based on the integration of the Doppler envelope (integral methods) are discussed. Theoretically, these algorithms can measure one component of the particle flux without errors. The residual bias induced by a wrong auto-calibration of the probe volume size is analysed and bounded in Section 2.

Under the common denomination of "validation errors" (in a broad sense), one refers to all those errors that change the number of particles counted by the PDA and alter the measure of flux and concentration. In particular, this includes phenomena that cause the multiple count of a single particle (e.g. burst splitting) (Van Den Moortel et al., 1997). Likewise, other errors that imply the loss or rejection of the signal generated by a particle are considered: the presence of several simultaneous particles in the measurement volume, signals with low SNR and others. In any case, different papers report strong bias in the flux integrated in the section normal to the stream preferential direction regarding the injected one (Dullenkopf et al., 1998; McDonell and Samuelsen, 1998). In the experimental part of this work, the measurements obtained by the PDPA are post-processed in order to reduce the underestimation of the flux. The developed correction is applicable to flows without breaking or particle evaporation.

Several experimental works about particle-laden jets or sprays include profiles of local axial flux or particle concentration. These data are applied to the description of the spatial particle distribution, calculations of dispersion parameters or comparisons with numerical models (Hishida and Maeda, 1990; Hishida et al., 1989, 1992; Prèvost, 1994; Heitor and Moreira, 1994; Sommerfeld, 1997).

In Section 3, a more complete characterisation procedure of the distribution and dispersion of spherical glass particles in a turbulent air jet is exposed. Particle local axial flux and velocity data supplied by a TSI-Aerometrics PDPA are post-processed to calculate a corrected axial flux (with minimised validation errors), the particle concentration and the radial flux. The measurement algorithm for the radial flux is one of the novelties of this paper. In this section also, a complete description of axial flux profiles (for five jet cross-sections and each size class) is expounded. The flux correction is made in order to reduce the measurement error as well as to improve the determination of particle dispersion parameters. Finally, several characteristic radii are proposed, as the radius that contains a percentage of the total injected flux and radius averaged over the jet cross-section.

2. Measurements on two-phase flows with multidirectional particle paths

For a one-component PDPA, concentration and particle flux calculation methods based on the counting of particles that cross the probe volume effective cross-section are suitable only with the one-directional particle movement hypothesis. Nevertheless, when particle path directions deviate from the direction of the velocity component measured by the PDPA, concentration and flux calculations are biased. This effect is called the directional bias by us. Particle trajectory deviations could be caused by several effects, as changes of the mean movement direction along the flow or a wide distribution of particle directions induced by the continuous phase turbulence (see Fig. 1).

When particles deviate significantly, methods that evaluate without bias flux and concentration of three-directional two-phase flows (derived from the first ones) must be used. So, only these integral methods are discussed in this paper. Following the technique developed by Sommerfeld, 1997, concentration and flux are calculated by means of the integration of an arbitrary function of the Doppler envelope over the effective probe volume. The effective probe volume size must be estimated by a previous calibration stage. Again, the calibration procedure could be affected by the directional bias effect. Errors induced by a wrong calibration are calculated and bounded.

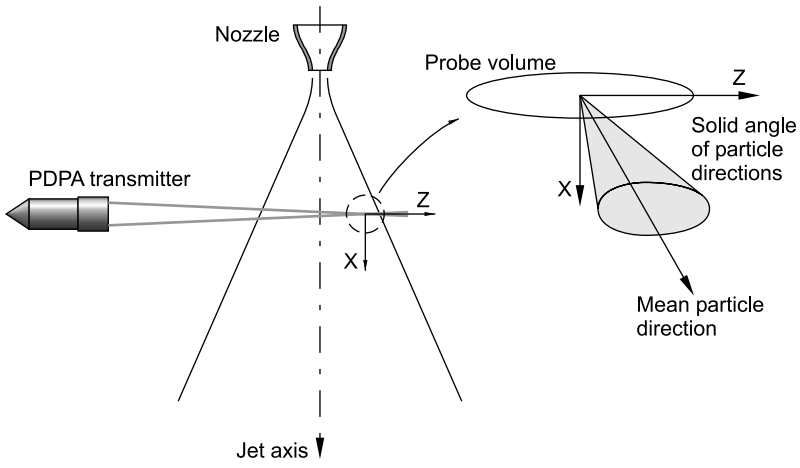

Fig. 1. Scheme of the directional bias phenomenon.

2.1. Calculation methods

The direct formulation based on the effective cross-section A_{ik} of particles of diameter D_i and path direction $\boldsymbol{n}_k$ is defined by these formulae:

$$\begin{aligned}\varphi_{Nxi} &= \frac{1}{\Delta t}\sum_{\forall k}\frac{N_{ik}}{A_{ik}}\left(\vec{\boldsymbol{n}}_x\vec{\boldsymbol{n}}_k\right) \equiv \text{Number flux for particles of } i\text{th size class},\\ C_{Ni} &= \frac{1}{\Delta t}\sum_{\forall k}\frac{1}{A_{ik}}\sum_{\forall j}\frac{1}{U_{ikj}} \equiv \text{Number concentration for particles of } i\text{th size class},\end{aligned} \tag{1}$$

where Δt is the measurement time, N_{ik} is the number of detected particles with direction $\boldsymbol{n}_k$ and size D_i that cross the cross-section A_{ik} and U_{ikj} is the velocity modulus of the jth particle of the class (i,k).

Sommerfeld and Qiu (1995) have developed a method derived from formulation (1) to evaluate particle concentration and flux efficiently and accurately. The work of Sommerfeld exposes the method by means of the integration of the Doppler envelope of particles that cross the probe volume. A more general formulation of the integral methods is proposed in this paper. The Generalised Integral Method (GIM) (Calvo et al., 2000) comprises all formulations of these methods and is expressed by means of an arbitrary function of the Doppler signal envelope. The calculations are given as:

$$\begin{aligned}C_{Ni} &= \frac{1}{\Delta t}\frac{\sum_{\forall kj} If_{ikj}}{\iiint_{\mathrm{Vol}_i} f(V_i(x,y,z))\,\mathrm{dVol}}\\ \varphi_{Nxi} &= \frac{1}{\Delta t}\frac{\sum_{\forall kj} U_{xikj}If_{ikj}}{\iiint_{\mathrm{Vol}_i} f(V_i(x,y,z))\,\mathrm{dVol}}\end{aligned} \qquad \text{with } If_{ikj} = \int_{t_{ikj}} f\left(V_{ijk}(t)\right)\mathrm{d}t, \tag{2}$$

where $V_{ikj}(t)$ is the Doppler envelope of the particle (i,k,j), If_{ikj} is the concentration integral parameter (a temporal integral of the function over the particle transit time, t_{ikj}), U_{xikj} is the measured velocity x-component and $\iiint_{\mathrm{Vol}_i} f(V_i)\,\mathrm{dVol}$ is a spatial integral over the effective probe volume for particle diameters D_i.

These integral methods are valid for any probe volume shape. For a PDA, the spatial distribution of the laser light intensity causes the probe volume to be an ellipsoid.

Once the arbitrary function $f(V)$ is defined and the probe volume Vol_i is calibrated for each point and particle size D_i, the temporal integral of each signal If_{ikj} can be easily evaluated, as well as the spatial integral. So, all the necessary information to evaluate the averaged concentration and flux can be obtained by a PDA of one component. This allows one to make the equipment easier and cheaper at the cost of a more complex signal processing system.

Integral methods developed on commercial systems can be formulated as particular cases of GIM. The Integral Value Method (IVM) (Sommerfeld and Qiu, 1995; Qiu and Sommerfeld, 1992) is obtained when the function of the Doppler envelope is equal to the envelope signal $f(V_{ikj}) = V_{ikj}$.

The Transit Time Method (TTM) (Zhu et al., 1993) is obtained from the GIM formulation when the function is equal to 1, $f(V) = 1$. As one can see easily, the concentration integral parameter is equal to the particle transit time t_{ikj}, and the spatial integral is the probe volume Vol_i.

Table 1
Particular integral methods for concentration and flux measurements

Measurement technique	Expressions
Integral Value Method (IVM) (Sommerfeld, 1993)	$C_{Ni} = \frac{1}{\Delta t} \frac{\sum_{\forall kj} \mathrm{Int}_{ikj}}{\int\int\int_{\mathrm{Vol}_i} V_i(x,y,z)\,\mathrm{dVol}}$ and $\varphi_{Nxi} = \frac{1}{\Delta t} \frac{\sum_{\forall kj} U_{Xikj}\mathrm{Int}_{ikj}}{\int\int\int_{\mathrm{Vol}_i} V_i(x,y,z)\,\mathrm{dVol}}$, where $\mathrm{Int}_{ikj} = \int_{t_{ikj}} V_{ikj}(t)\,\mathrm{d}t$ and $\int\int\int_{\mathrm{Vol}_i} V_i(x,y,z)\,\mathrm{d}V = \frac{\pi r_0^2 L_Z}{2} V_T \left[\exp\left(2\frac{r_{Ti}^2}{r_0^2}\right) - 1\right]$
Transit Time Method (TTM) (Zhu et al., 1993)	$C_{Ni} = \frac{1}{\Delta t} \frac{\sum_{\forall kj} t_{ikj}}{\mathrm{Vol}_i}$, where $\mathrm{Vol}_i = \pi r_{Ti}^2 L_Z$

TTM has been implemented on the TSI-Aerometrics PDPA. Reduced expressions of these particular methods are given in Table 1.

2.2. Auto-calibration techniques

Integral methods and GIM expressions provide efficient concentration and flux evaluation algorithms. Indeed, all information can be obtained by a PDA of one component. However, as shown in Fig. 2, probe volume geometry must be known to do the spatial and temporal averaging process.

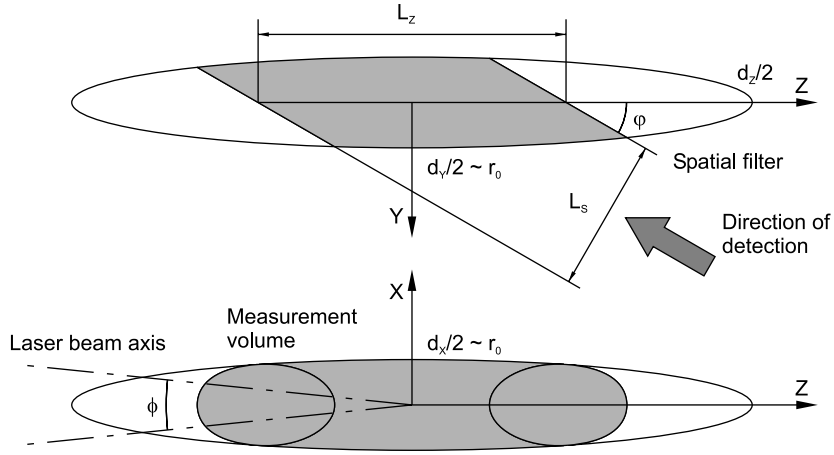

Fig. 2. Probe volume geometry.

The particle signal level depends on several variables, such as the particle diameter D_i, photomultipliers excitation, system gain, reception optics, light attenuation through the flow and others. This complex dependency suggests to make a probe volume calibration for each measurement point. It must be noted that for a measurement point and a fixed trigger level V_T, the probe volume radius is a function only of the particle diameter $r_T(D_i)$. The probe volume length L_Z is determined only by the reception optics.

Different auto-calibration methods for r_{Ti} that use measured particle signal parameters have been developed for each PDA model.

A very simple and stable method is implemented on the PDPA of TSI-Aerometrics (Zhu et al., 1993) used in the experimental part of this work. It estimates the probe volume radius as one half of the largest burst spatial length $L_{ikj} = U_{ikj}t_{ikj}$.

2.3. Evaluation and bounding of directional bias

When particle directions are not the ones assumed by the concentration calculation methods and auto-calibration stage, these techniques are affected by the named directional bias. These errors have been evaluated for the most common measurement systems and one-directional particle motion by Calvo et al. (2000). In this paper, only TTM and Aerometrics calibration errors are given in order to bound the Aerometrics PDPA measurement bias.

For a PDPA of one component and a one-directional flow with particle path direction $\boldsymbol{n}(\theta, \psi)$ (see Fig. 3), Aerometrics' calibration measure a biased probe volume radius r_{TiM}. It is related to the actual one r_{Ti} by the expression

$$r_{TiM} = r_{Ti}|\sin\psi|. \tag{3}$$

This error could happen when particles have a directional distribution with a maximum deviation of $\pi/2 - \psi_{\min}$.

The decrease of the estimated radius creates a bias of the concentration calculated by TTM (Calvo et al., 2000) equal to

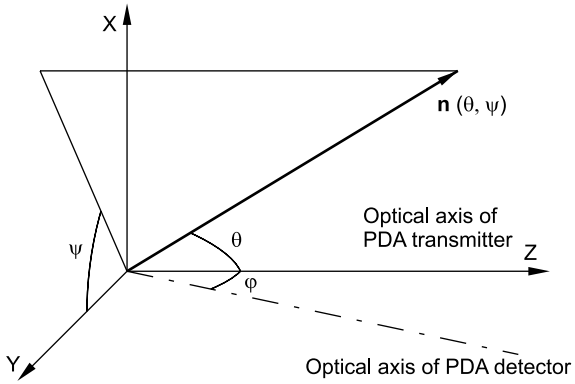

Fig. 3. Definition of particle path direction $\boldsymbol{n}(\theta, \psi)$.

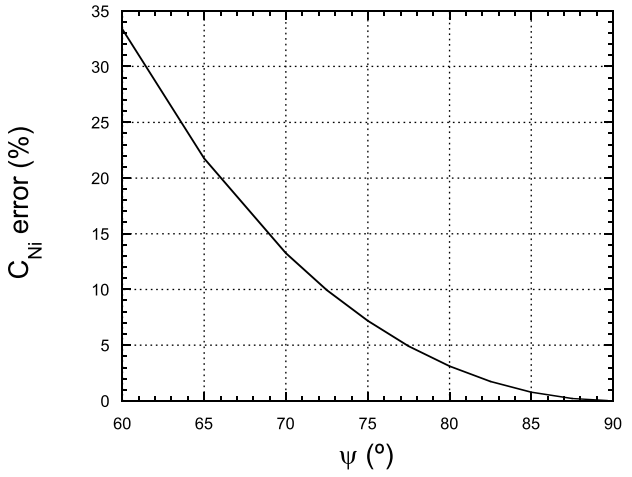

Fig. 4. TTM concentration bias vs. path direction.

$$\varepsilon_{Ci} = \frac{r_{Ti}^2}{r_{TiM}^2} - 1. \tag{4}$$

Error ε_{Ci} is plotted vs. the angle ψ in Fig. 4. It must be noted that if the probe volume calibration is accurate, TTM (and GIM formulation) have no directional bias. This error evaluation is used to bound measurement errors of flows with a known particle direction distribution. The deviation $\pi/2 - \psi_{\min}$ is estimated as the angle such that there is a significant percentage of particles in the interval of $\psi(\psi_{\min}, \pi/2)$.

3. Experimental study of a particle-laden jet

3.1. Experimental set-up

Concentration, particle flux and other variables have been measured in an axisymmetric air jet laden with glass spheres of density $\rho_P = 2450$ kg/m^3. The jet is discharged through a pipe of about 1 m length ending in a nozzle of diameter $D = 12$ mm, area contraction ratio $r_{Ao/Ai} = 5.14$ and length 75 mm. The detail of the nozzle geometry is shown in Fig. 5.

Airflow is measured by an orifice meter and controlled by a computer that drives a pneumatic valve. In order to measure the gas velocity, air is seeded with alumina powder whose mean diameter is 0.5 μm. A vibrating device controls carefully the injection of spherical particles with an error of 1.5%. Both air and glass spheres are injected through the upper intake of the pipe. The flow develops in a square transparent chamber of dimensions $480 \times 480 \times 1000$ mm^3. A low velocity secondary air flow (co-flow) of velocity 0.2 m/s is supplied into the confinement chamber. A detailed scheme of the chamber, reference and air control appears in Fig. 6.

Particle velocity and diameter are measured by means of a two-component TSI-Aerometrics PDPA with FFT signal processors mod. 3100. Light to the optical transmitter and from the

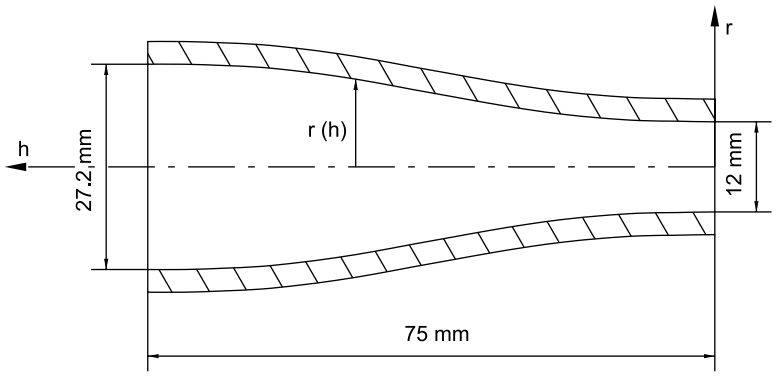

Fig. 5. Nozzle geometry.

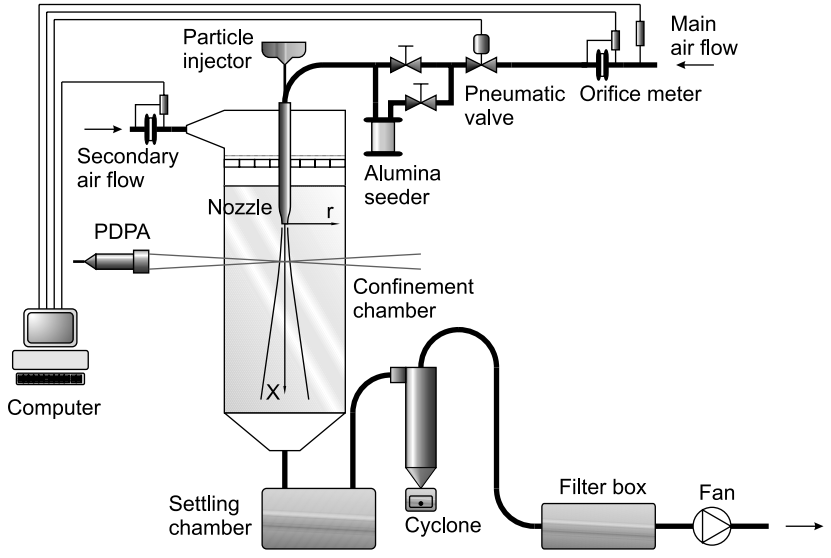

Fig. 6. Scheme of the experimental facility and reference system (x, r).

receiver is conducted by an optical fibre. A 2D mechanism controlled by computer moves the whole optical system. Forward scattering is detected, with direction detection at 30° from the transmitter optical axis.

The PDPA software measures particle flux and concentration by means of the TTM algorithm. The measurement volume calibration is performed by the Aerometrics auto-calibration.

The experimental study has been carried out in a domain extending from the exit nozzle to 10 nozzle diameters downstream ($10D$). This zone includes the initial development of the two-phase jet. Flow magnitudes have been measured in sections $x^+ = x/D = 0.5$; 2.5; 5.0; 7.5 and 10. Particle

concentration and flux are obtained for five diameter classes from 50 to 100 μm with width equal to 10 μm. For each measurement point, the number of samples is greater than 15,000 particles in order to obtain more than 1000 measured particles for each particle diameter class. The characteristic Stokes number (St) for the air–particle interaction goes from 6 to 30. The flow time scale used to estimate the Stokes number is the characteristic time of turbulent large scales.

All measurements of dispersal phase quantities (e.g. velocity, size, flux and concentration of glass spheres) have been made in the absence of tracers for the gas phase (not alumina powder present at all).

Just the gas velocity field measurements of the two-phase jet have been made seeding the air with alumina. These measurements are included in Figs. 8 and 22 to state the study conditions. Since there is no glass spheres of diameter less than 10 μm (see Fig. 7), signals with measured size under 10 μm are considered as alumina Doppler bursts.

Jet injection conditions are defined by an air velocity of 15 m/s and a particle–air mass ratio of $r_M = 0.3$. Sphere size distribution, air and dispersed phase velocity profiles and particle flux at the nozzle exit are given in Figs. 7–9. More than the 90% of particles are quite and perfectly spherical.

3.2. Particle flux and concentration measurement procedure

Starting from the measurements of the local volume axial flux of each particle size class φ_{Xi} (supplied by the PDPA system), a procedure to obtain the most complete description of particle distribution in the studied domain is developed. The corrected volume local axial flux g_{xi}, the particle volume concentration C_{Vi} and the corrected volume radial flux g_{ri} are obtained for each particle diameter class. The measurement procedure is detailed in the following paragraphs. A test of consistency has been made through the comparison of two different evaluations of radial flux.

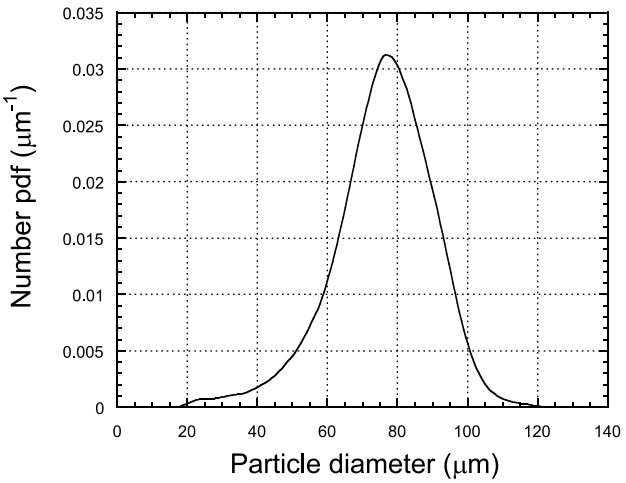

Fig. 7. Number pdf of particle size.

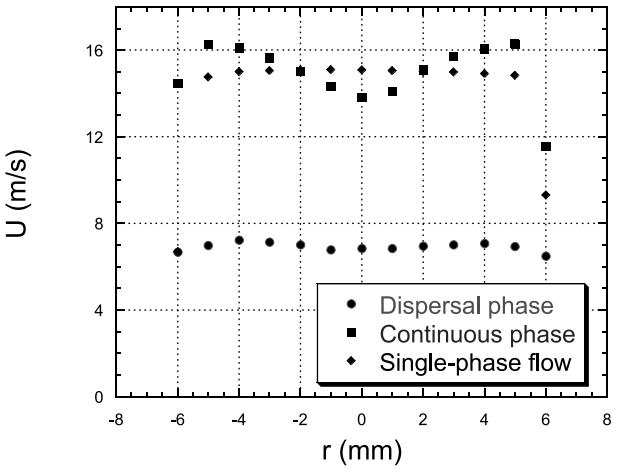

Fig. 8. Exit velocity profiles ($x/D = 0.5$).

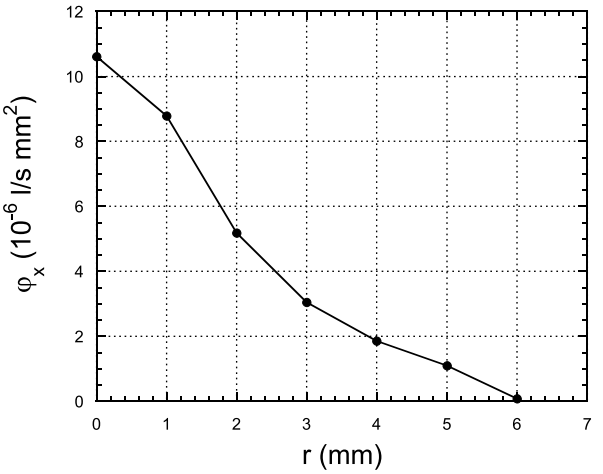

Fig. 9. Profile of volume axial flux at nozzle exit ($x/D = 0.5$).

3.2.1. Axial flux

Particle axial flux φ_{Xi} has been measured over the radius of each jet cross-section. The most exterior point of the jet periphery corresponds to a measurement time longer than 30 min. Flux profiles have been tested to detect problems. In particular, the particle mass conservation along the jet is examined. The total mass flux of particles with size D_i throughout each jet section $x = x_j$ is calculated as the integral of the local axial flux profile φ_{Xi} over the section (applying the axisymmetric hypothesis). The integrated mass flux over the section x_j is compared with the controlled injected mass per unit time G_i. This allows us to detect an axial flux underestimation. Particle mass conservation for each particle diameter must happen in this flow, without particle breaking and mass transfer between both phases (glass spheres and air).

There are several effects that alter the flux and concentration measurements, as:

(i) Losses of signal due to an inaccurate validation process:
  (a) Signals of low SNR.
  (b) Multiparticle signals.
(ii) The "burst splitting" phenomenon.
(iii) The "directional bias" effect.

Flow characteristics as particle concentration, light path length crossing the flow, the probe volume size and other PDA operation parameters set these effects.

Some of the error sources listed before have been estimated. Thereby, the error in the concentration due to the "directional bias" is less to one per cent in the most unfavourable point. On the other hand, the burst splitting phenomenon amounts to less than three per cent of the signals, according to thorough inspection of the acquired signals.

The relative weight of all effects can cause an over or underestimation. In this two-phase jet, the axial flux is underestimated by around 20%. This deficit is slightly different in each cross-section, but it goes from 26% at the exit section ($x/D = 0.5$) to 15% at the section $x/D = 10$.

Some of the errors that could modify the profile shape along the cross-section (burst splitting, multiparticle signals, directional bias) generate a low bias value. Other validation errors that also depend on the concentration could alter the flux profile shape. Because there is not available, at the present day, suitable algorithms to correct all those effects, it is not possible to evaluate the exact profile. Under these conditions, a post-processing which equates the integrated mass flux over each section to the injected mass rate is applied (for each particle size class) in order to correct the local flux profiles. This correction can be used in flows with low or medium single phase density and without breaking particles or mass transfer between phases. On the other hand, a test of the measurement quality is made in this paper, comparing two ways to obtain the integral radial flux.

The measurements of axial flux φ_{xi} of the ith size class have been normalised with the injected volume rate G_i. The normalisation coefficients K_{ij} of each transversal section of position $x = x_j$ are obtained as

$$G_i = K_{ij} \int_0^\infty \varphi_{xi}(r, x_j) 2\pi r \, \mathrm{d}r. \tag{5}$$

The local flux has been corrected, using the K_{ij} coefficients.

$$g_{xi}(r, x_j) \equiv K_{ij} \varphi_{xi}(r, x_j). \tag{6}$$

In the attached graphs, the results of the flux normalisation for the local axial flux in the transversal section at $x = 2.5D$ from the nozzle are shown. Radial semiprofiles of the normalised axial local flux are plotted in Fig. 10 for each ith size class. Fig. 11 shows the normalisation coefficients at this section. Profiles of corrected local axial flux are compared with the direct results of the total particle distribution in Fig. 12. In this section, the flux deficit before normalisation is equal to 19%.

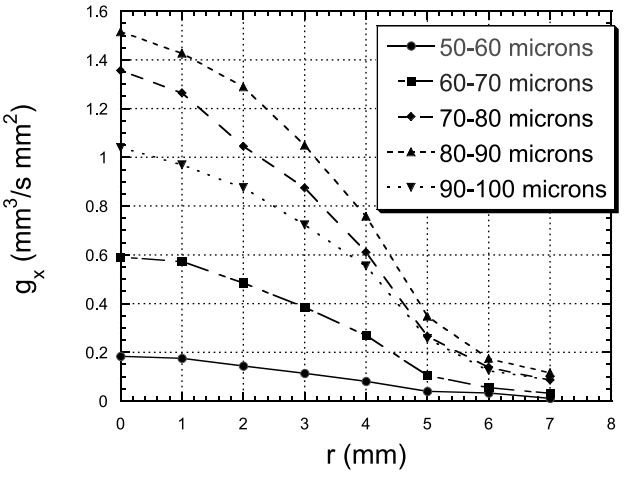

Fig. 10. Normalised axial flux profiles of each particle size class at $x/D = 2.5$.

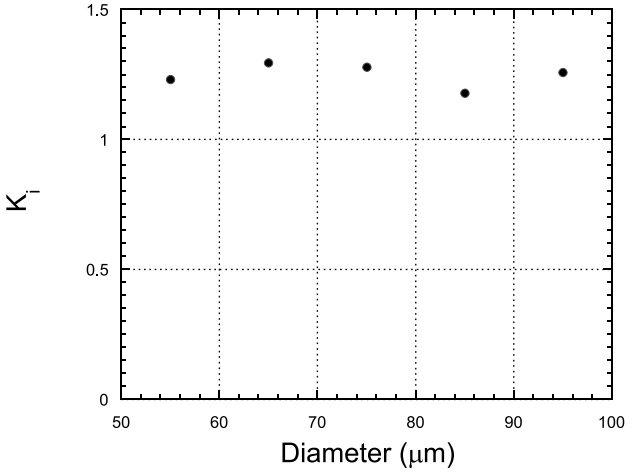

Fig. 11. Normalisation coefficients at $x/D = 2.5$.

3.2.2. Particle concentration

Particle flux and concentration are related by the particle velocities. Indeed, flux can be calculated as the concentration multiplied by an averaged velocity. This averaged velocity is the spatial main velocity $\overline{U_{Xi}}|_S$. From the GIM formulation, the ratio flux/concentration is equal to

$$\frac{\varphi_{xi}}{C_{Vi}} = \frac{\sum_{\forall kj} U_{xikj} If_{ikj}}{\sum_{\forall kj} If_{ikj}}. \tag{7}$$

As one can see, each particle velocity is weighted by a factor proportional to the concentration integral parameter. For the TTM, the particle spatial velocity is the one corrected by the transit time (Eq. (8))

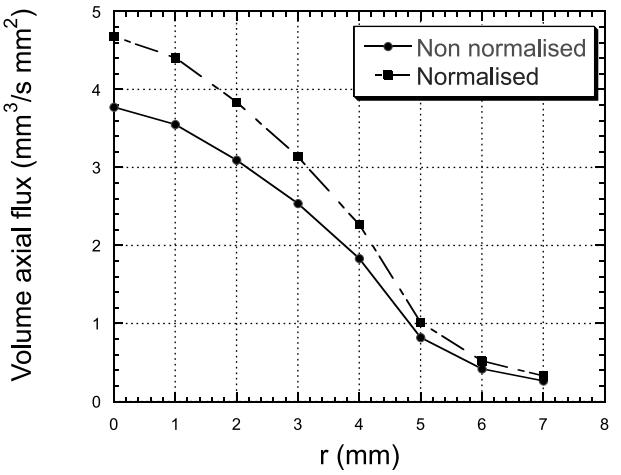

Fig. 12. Normalised and non-normalised flux profiles at $x/D = 2.5$.

$$\frac{\varphi_{xi}}{C_{Vi}} = \frac{\sum_{\forall kj} U_{xikj} t_{ikj}}{\sum_{\forall kj} t_{ikj}} = \overline{U_{xi}}|_S. \tag{8}$$

It must be noted that the total volume concentration and flux are obtained as the sum of all size class concentrations and flux.

$$C_V = \sum_{\forall i} C_{Vi} \quad \text{and} \quad \varphi_x = \sum_{\forall i} \varphi_{xi}. \tag{9}$$

Using this method, the corrected concentration is calculated from the normalised volume flux g_{xi} instead of the non-normalised. Corrected volume concentration profiles of the section $x/D = 2.5$ are plotted in Fig. 13.

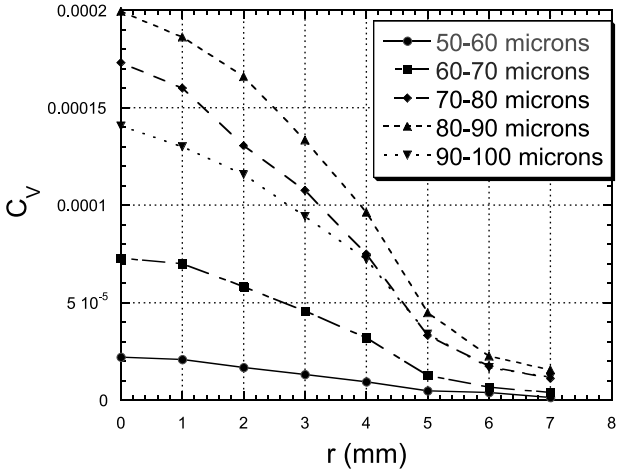

Fig. 13. Corrected volume concentration profiles of the section $x/D = 2.5$.

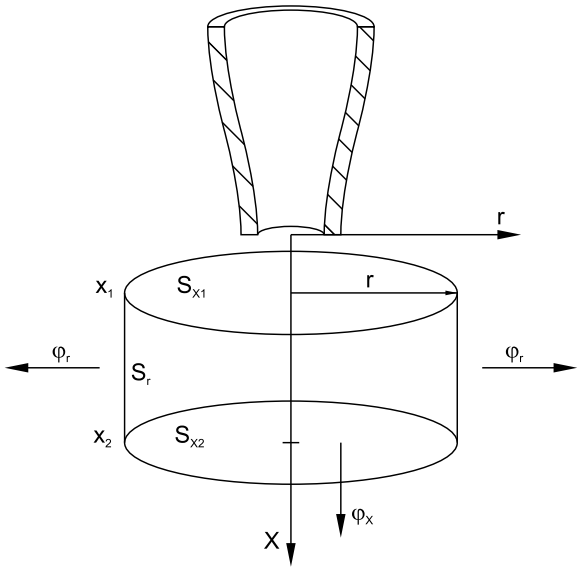

Fig. 14. Cylindrical box used for radial flux estimation.

3.2.3. Radial flux

Two estimations of radial flux have been made. In the first evaluation, a balance of particle conservation is applied in cylinders. These cylinders are centred on the jet axis and bounded between two transversal sections as Fig. 14 shows. In the second evaluation, the relation with local flux, concentration and mean velocity corrected by transit time is used.

The balance in the cylinder of radius r between transversal sections x_1 and x_2 leads to the following expression

$$\Phi_{ri}(r,x_1,x_2) = \Phi_{xi}(r,x_1) - \Phi_{xi}(r,x_2) \quad \text{with } \Phi_{xi}(r,x_j) \equiv \int_0^r \varphi_{xi}(\rho,x_j)2\pi\rho\,\mathrm{d}\rho, \tag{10}$$

which represents the evaluation of the integrated volume axial flux over a circle of radius r, using the approximation of axial symmetry, at the transversal section x_j. Radial and axial integral fluxes obtained from the normalised axial flux g_x (instead of the non-normalised one φ_x) are named G_r and G_x, respectively.

In the second estimation, the local volume radial flux is calculated with the next expression:

$$\varphi_{ri} = C_{Vi}\overline{U_{ri}}|_S. \tag{11}$$

Again, the local radial flux calculated with normalised axial flux g_x is named g_r.

In the approximation of axial symmetry and the linear evolution of the radial local flux with x, the integrated radial flux $\Phi_{ri}(r,x_1,x_2)$ over lateral surface is expressed by the expression

$$\begin{aligned}\Phi_{ri}(r,x_1,x_2) &= \int_{x_1}^{x_2} \varphi_{ri}(r,x)2\pi r\,\mathrm{d}x \\ &\approx \varphi_{rmi}(r,x_1,x_2)2\pi r(x_2-x_1) \quad \text{with } \varphi_{rmi}(r,x_1,x_2) = \frac{\varphi_{ri}(r,x_1)+\varphi_{ri}(r,x_2)}{2}.\end{aligned} \tag{12}$$

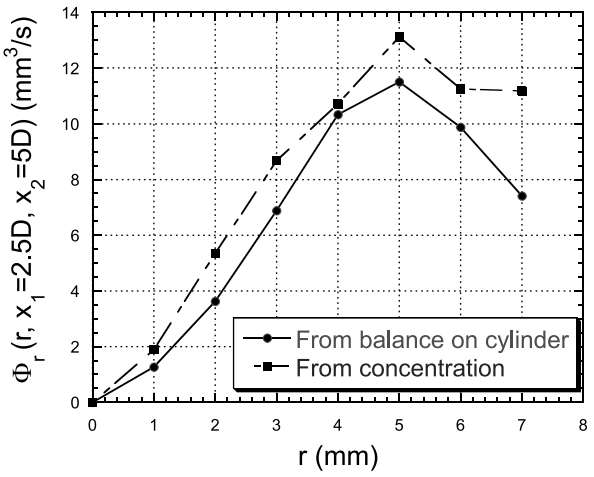

Fig. 15. Integrated radial flux of the 70–80 μm size class before normalisation.

The two evaluations of the volume radial flux integrated over the lateral surface of cylinders between transversal sections at $x_1 = 2.5D$ and $x_2 = 5D$ (Eqs. (10) and (12)) are shown in Fig. 15 for the non-normalised results and in Fig. 16 for the normalised case. Both figures display data for 70–80 μm size class. Also, plots of the mean radial velocity corrected by transit time for each particle size are given in Fig. 17.

The integrated radial flux (evaluated with Eq. (10) since it is more stable) exhibits some evolution characteristics with the radius: in the internal layers, it is growing almost quadratically; presents an inflexion point and a maximum; and is decreasing in the furthest radius.

The comparison of the evaluations of integrated radial flux, with and without normalisation, leads to three conclusions:

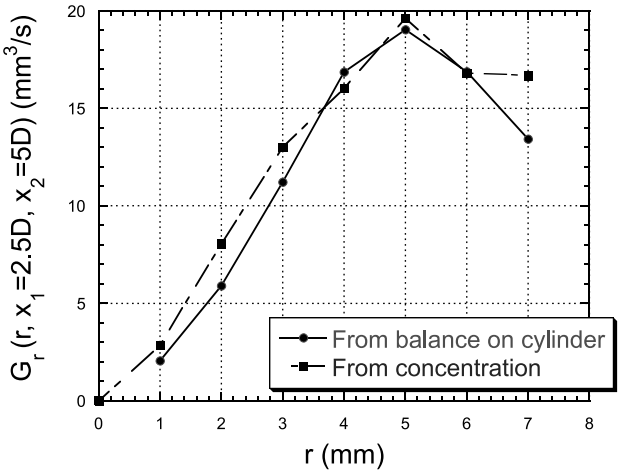

Fig. 16. Integrated radial flux of the 70–80 μm size class after normalisation.

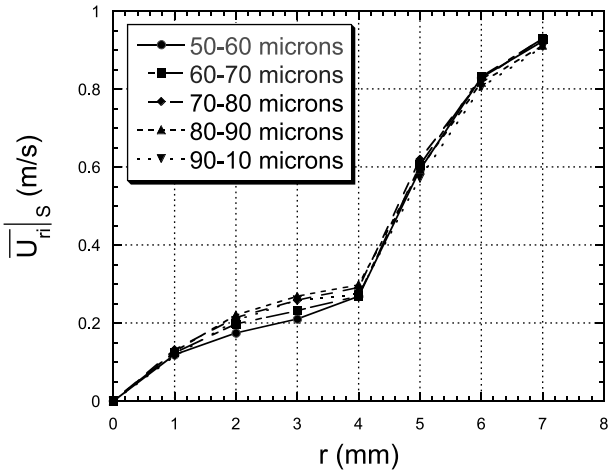

Fig. 17. Mean radial velocities corrected by transit time at section $x/D = 2.5$.

(i) The particles balance in a cylinder and the evaluation based on the concentration and mean radial velocity give a similar evolution. Numerical differences are not important if one bears in mind the particular approximations considered.
(ii) The differences between both estimations observed in the non-normalised case are caused by different percentages of non-validated particles. Indeed, if the percentage of lost signals were the same for sections $x_1 = 2.5D$ and $x_2 = 5D$, the error between both estimations (expressed as a percentage) would be equal for the normalised and non-normalised cases. The developed post-processing corrects this effect.
(iii) The agreement between both evaluations is better in the normalised case.

These conclusions are considered as a test of consistency and they prove the validity of the measurements and of the subsequent treatment.

3.3. Evolution of the axial flux

The detailed study of the spatial distribution of particles in the jet development zone has been made by means of the particle axial flux. Five transversal sections $x^+ = x/D = 0.5$; 2.5; 5; 7.5 and 10 have been studied. In this section, the evolution of the local axial flux profiles, the flux integrated on coaxial circles centred at the jet axis and the curves of the particle distribution and dispersion parameters are presented successively. Likewise, interpretations of these evolutions (based on the action of several particle dispersion mechanisms) are suggested.

3.3.1. Local axial flux

The evolution of the normalised axial flux profile $g_x(r)$ for all particles and each studied cross-section is shown in Fig. 18. Non-dimensional profiles are given in Fig. 19. The non-dimensional flux is defined as $g_x^+(r) = g_x/g_{x0}$ with $g_{x0} = g_x(r = 0)$. For the radial co-ordinate, the non-dimensionalisation parameter is the radius $R90$ of the circle that contains the 90% of the total

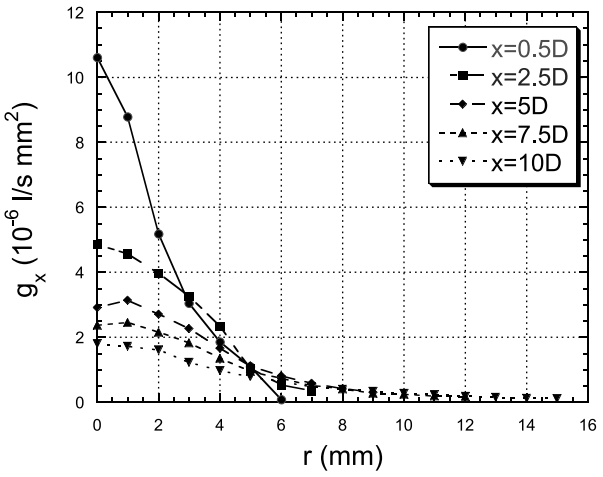

Fig. 18. Profiles of corrected volume axial flux for overall distribution.

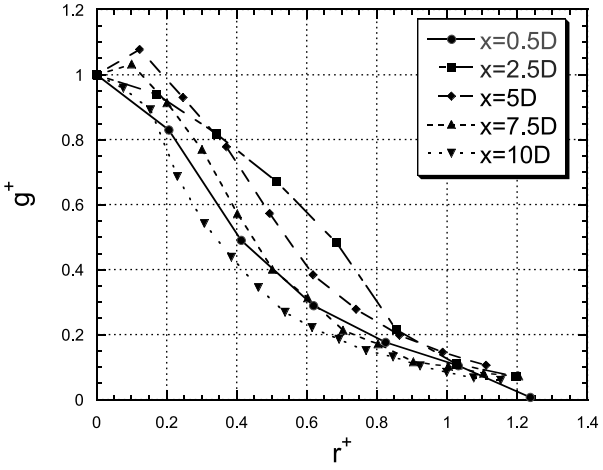

Fig. 19. Non-dimensional profiles of volume axial flux for overall distribution.

particle flux $G_x(R90) = 0.9 \cdot G_x(r \to \infty)$. So, $r^+ = r/R90$. The comparison of dimensionless flux profiles permits to establish two evolution zones:

(i) In the zone close to the exit nozzle, the central wedge-shaped curve smoothes down quickly, and the flux becomes wider in the inner jet layers, despite the particle acceleration in this flow zone. The radius r_{50}^+ (defined as the non-dimensional radius where the local axial flux g_X is equal to a half of the axial flux at $r = 0$) changes form 0.41 at $x/D = 0.5$–0.68 at $x/D = 2.5$. Particles with a strong directional dispersion at the exit nozzle (caused by particle impacts on the nozzle wall) are nearly parallel at locations downstream.
(ii) From the cross-section located at $x = 5D$ onwards the profiles show a different evolution. The maximum dimensionless flux profile slope grows and moves to smaller non-dimensional

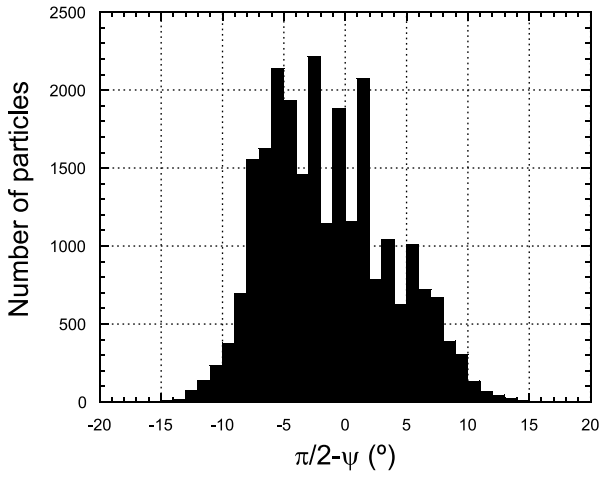

Fig. 20. Particle directional distribution at the point $r = 0$; $x/D = 0.5$.

radius as the x coordinate increases. The shape of the profiles gets narrower again. Thus, r_{50}^{+} is equal to 0.55, 0.45 and 0.33 at sections $x/D = 5$; 7.5 and 10, respectively.

The radial dispersion of the particles in the first zone (close to the nozzle) seems to be dominated by the jet exit conditions. Particles with large Stokes number and wide directional distribution at the exit nozzle (caused by particle impacts on the nozzle wall) are nearly parallel at locations downstream. This phenomenon is called the directional classification by us. This evolution is shown in the particle directional distribution (Figs. 20 and 21) of the points $r = 0, x/D = 0.5$ and $r = 0, x/D = 7.5$, respectively (García, 2000). The flux profile expansion of this zone is associated with the directional classification. The rebounds of particles on the nozzle wall

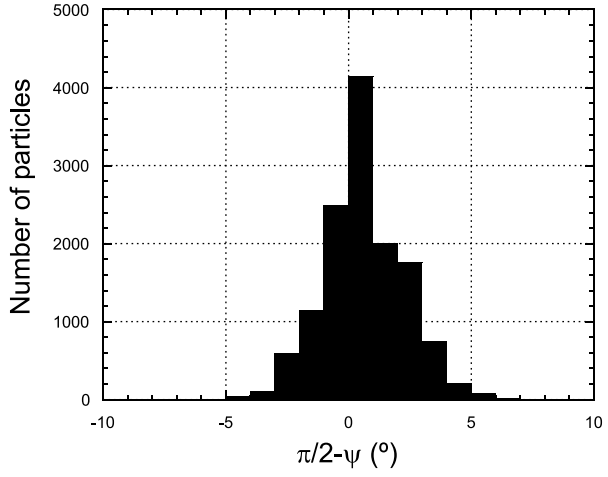

Fig. 21. Particle directional distribution at the point $r = 0$; $x/D = 7.5$.

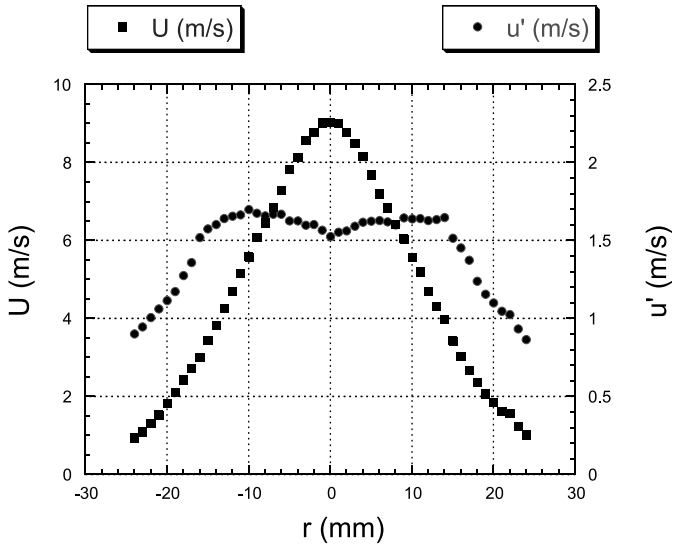

Fig. 22. Mean gas velocity and RMS profiles at section $x/D = 10$.

are discussed in several works about jets (Prèvost, 1994; Hardalupas et al., 1989). In a jet with a similar nozzle, Longmire and Eaton (1992) explains the particle focalisation at the jet axis as a consequence of the impacts on the nozzle. This generates the pointed local flux profile at the nozzle exit section.

In the second zone (from $x/D = 5$ onwards) the gas axial velocity profile evolves towards a nearly Gaussian shape in section $x/D = 10$ (see Fig. 22). The profile evolution of local flux is caused by several simultaneous phenomena. The aerodynamic interaction with the mean gas flow induces zones of particle acceleration and deceleration. A series of weak action factors that generate radial transport are: the turbulence of continuous phase (with high Stokes number values), the rebounding crash between particles and even the Magnus–Saffman effect acting on rotating particles in zones of high gas radial gradient (Saffman, 1965). It is observed that the evolution of axial flux profiles is smoothed and regularised towards the end of the domain studied. It is not expected to find adequate scales that permit us to find self-preservations in the domain. Despite this, it has been tried to make the radial position be non-dimensional with the length scale $L_D = U_{gx}(r = 0) \cdot \tau_P$ inspired in the works of Lázaro and Lasheras (1992a,b) about a shear layer. In the definition of L_D, τ_P is the particle response time and U_{gx} is the axial velocity of the gas. The result is negative.

3.3.2. Integrated axial flux

Integrated axial flux $G_x(r)$ calculated with the normalised local flux $g_x(r)$ is shown in Fig. 23 for each measured jet cross-section and all particles. Integrated flux has been made dimensionless with its maximum value $G_x^+(r) = G_x(r)/G_{x\max}$. It must be noted that the maximum normalised integral flow is equal to the total injected particle volume rate $G_{x\max} = G_{\text{Total}} = \sum_{\forall i} G_i$.

The final radius with presence of particles (in each section $x = x_j$) is defined as the radial position where the measurement time is longer than 30 min. So, the measurements are truncated in

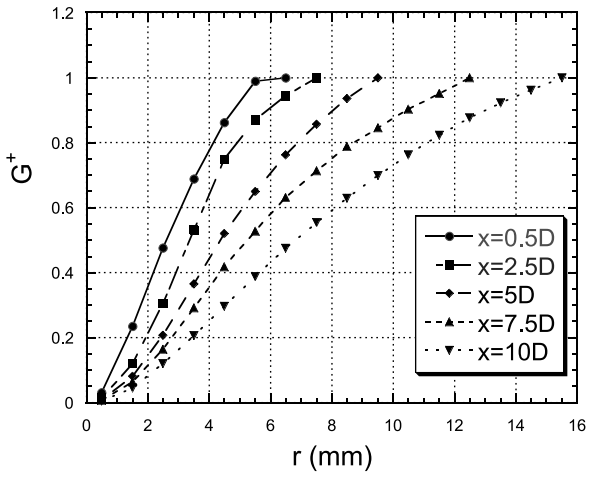

Fig. 23. Profiles of non-dimensional integrated axial flux.

the referred final point. This kind of truncation has been used by other researches (Hishida and Maeda, 1990; Prèvost, 1994; Heitor and Moreira, 1994). On the other hand, the following considerations about the truncation can be established

(i) In the first section $x/D = 0.5$ (limited by the solid walls of the nozzle and the focalisation effect), the deficit of the integrated total flux reaches a maximum value equal to 26%. Therefore, the loss of particles cannot be attributed to the truncation and the non-measured external radial flux, but to problems in the signal validation.
(ii) The contribution of the following annulus to the total integrated flux is, in all cases, very inferior to the non-corrected flux deficit.
(iii) Finally, the outstanding improvement of the radial flux comparison calculated by both methods (see Section 3.2) when the correction of local fluxes is used validates the usefulness of the process.

Integral flux profiles reveal again the two zones of spatial distribution evolution. On the other hand, characteristic radii RX that describe the particle spatial distribution are obtained directly. RX parameter is defined as the radius of the circle that contains the X% of the total flux. In this study, only $R10$, $R50$ and $R90$ have been used. These radii describe the growth of the jet core, the middle layer and the jet edge. Their evolution along jet axis is shown in Fig. 24. It must be noted that if particles had straight paths with the same origin, $RX(x)$ would be straight lines. The figure shows that $R90$ has a monotonous evolution along x. At the beginning, its slope grows and from station $x/D = 5$ onwards it evolves linearly. $R10$ and $R50$ show a more complex evolution.

3.3.3. Dispersion radius

A few works (Prèvost et al., 1996; Hishida et al., 1992; Ishima et al., 1993) associate a particle global dispersion parameter with each section of the flow. These parameters are defined as moments of the radius weighted by the particle distribution fields (e.g. flux or concentration).

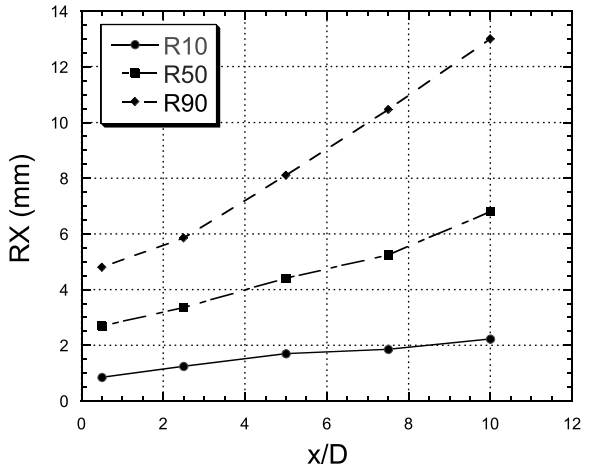

Fig. 24. Integral radii development.

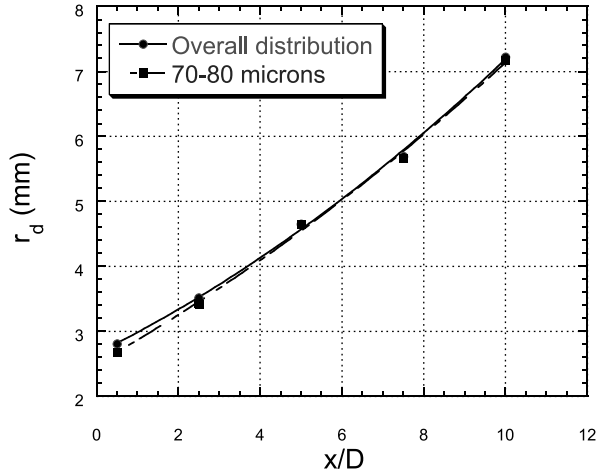

Fig. 25. Dispersion radius development of overall particles and 70–80 μm size class.

In this work, the first moment of the radial coordinate weighted by the local axial flux is calculated as a characteristic parameter of particle dispersion. The named dispersion radius r_{di} is defined for each particle size as

$$r_{di} = \frac{\int_0^\infty r^2 \varphi_{xi}\,\mathrm{d}r}{\int_0^\infty r \varphi_{xi}\,\mathrm{d}r}. \tag{13}$$

Dispersion radius for overall particle sizes is defined by using the total volume local flux g_x. It is plotted vs. x in Fig. 25.

4. Conclusions

An experimental study of particle dispersion has been made with phase Doppler technique in an air jet loaded with glass spheres. The used gas-to-particle mass ratio is 0.3. The study is carried out in the first development zone of an axisymmetric jet, created by air exiting from a nozzle.

First of all, the integral methods of flux and concentration evaluation (adequate for three-dimensional movement of particles) are revised. It is remarked that under optimum conditions and with efficient auto-calibration techniques (such as the implemented in the PDPA mod. 3100 of Aerometrics) the bias introduced can be negligible. In this way, the errors in the concentration flux measurement are limited to:

(i) The ones introduced by the errors of the particle parameter measurements (as particle velocity, diameter, transit time, etc.)
(ii) The so-called "signal validation errors" of multiple origin, with difficult solution and responsible to a great extent for the measurement imprecisions.

The characteristics of the studied flow (defined by the injection conditions) lead to: (i) a strong slip between continuous and dispersal phases; (ii) the initial focusing of particles at the jet axis; (iii) a medium-high range of Stokes number (form 6 to 30, referred to the mean particle diameter).

A methodology of maximum efficiency to characterise the spatial distribution of the flux and concentration fields through the processing of the measured local axial flux by size classes has been established. As a first step, the profiles of axial flux are normalised with the injected mass rate for each size class in all measured transversal sections. The normalisation reduces the error caused by low validation rates of signals and improves the consistency of the parameters of jet development. This correction is applicable to flows with a predominating direction, medium or low phase concentration, without breaking particles and in the absence of mass transference between both phases. Then, the particle concentration is obtained from the corrected axial flux and the axial velocity results for each size class.

Lastly, the concentrations of each size class together with particle radial velocity data generate results for the local radial flux. The results of the obtained radial flux are integrated over the lateral surface of coaxial cylinders centred at the jet axis. They are compared with the calculated values by means of the particle conservation applied to these cylinders. The outstanding agreement obtained in the comparison of both estimations of the integrated radial flux is considered as a validation of the axial flux correction.

The detailed study of the spatial distribution of particles is made with the axial flux. The radial profiles have been analysed in dimensional $g_x(r)$ and non-dimensional $g_x^+(r^+)$ forms. There are two sub-zones of axial development:

(i) Close to the nozzle, the focalised and pointed profile shape shows a quick smoothing. A strong radial particle transport in the central region is produced by the exit conditions.
(ii) From the $x/D = 5$–10 section, the profile development changes towards a new pointed shape. On the one hand, the aerodynamic drag of the mean gas flow acts and the gas mean ve-

locity tends to a Gaussian profile. On the other hand the radial transport is slightly influenced by the gas turbulence (with Stokes numbers higher than 6.4), the collisions between particles and even the Magnus effect. In the domain studied, adequate scales that make self-preserving flux profiles have not been found.

The integration over transversal sections of the flux inside circles of radius r, centred in the jet axis, is used to get the characteristic radii ($R10$, $R50$, and $R90$). In this way, it is possible to characterise the development of the core, body and edge of the jet. Finally, the mean radius, weighted with the local axial flux, is a parameter to characterise the whole dispersion.

Acknowledgements

The authors would like to acknowledge the support for this work given by the Spanish Department of Scientific and Technological Research (CICYT) through projects IN95-0219 and AMB96-0427-C03-03. J.A. García has been supported by CONAI grants BIT 41/93 and E. Calvo is supported by the Education and Culture Ministry grants 1999-01-19N AP98.

References

Calvo, E., García, J.A., Cerecedo, L.M., García-Palacín, I., Aísa, L.A., 2000. Particle concentration and mass flux measurements with PDA: a study about methods and errors. In: Proceedings of the 16th European Conference on Liquid Atomization and Spray Systems, Darmstad, Germany, September 11–13.

Dullenkopf, K., Willman, M., Witting, S., Schöne, F., Stieglmeier, M., Tropea, C., Mundo, C., 1998. Comparative mass flux measurements in sprays using a patternator and the phase-Doppler technique. Part. and Part. Syst. Characterization 15, 81–89.

Durst, F., Umhauer, H., 1975. Local measurements of particle velocity, size distribution and concentration with a combined laser Doppler particle sizing system. In: Proceedings of the LDA-Symposium, Copenhagen, Denmark, August 25–28.

García, J.A., 2000. Estudio experimental de un chorro bifásico axilsimétrico: Medidas de concentración e intensidad de flujo de partículas; características de dispersión. Ph.D. Thesis, Universidad de Zaragoza, Spain.

Hardalupas, Y., Taylor, A.M.K.P., Whitelaw, J.H., 1989. Velocity and particle-flux characteristics of turbulent particle-laden jets. Proc. R. Soc. Lond., 31–78.

Heitor, M.V., Moreira, A.L.N., 1994. Experiments on polydisperse two-phase turbulent jets. ICLASS 94; XI-6; Rouen, France.

Hishida, K., Nakano, H., Maeda, M., 1989. Turbulent flow characteristics of liquid–solid particle confined jet. In: International Conference on Mechanics of Two-Phase Flows, pp. 209–214.

Hishida, K., Maeda, M., 1990. Application of laser Doppler anemometer to dispersed two-phase jet flow. Part. and Part. Syst. Characterization 7, 152–159.

Hishida, K., Ando, A., Maeda, M., 1992. Experiments on particle dispersion in a turbulent mixing layer. Int. J. Multiphase Flow 18, 181–194.

Ishima, T., Hishida, K., Maeda, M., 1993. Effects of particle residence time on particle dispersion in a plane mixing layer. J. Fluids Eng. 115, 751–759.

Lázaro, B.J., Lasheras, J.C., 1992a. Particle dispersion in the developing free shear layer. Part 1. Unforced flow. J. Fluid Mech. 235, 143–178.

Lázaro, B.J., Lasheras, J.C., 1992b. Particle dispersion in the developing free shear layer. Part 2. Forced flow. J. Fluid Mech. 235, 179–221.

Longmire, E.K., Eaton, J.K., 1992. Structure of a particle-laden round jet. J. Fluid Mech. 236, 217–257.
McDonell, V.G., Samuelsen, G.S., 1998. Application of two-component phase interferometry to the measurement of particle size, mass flux, and velocities in two-phase flows. In: 22th Symposium (International) on Combustion/The Combustion Institute, 1988, pp. 1961–1971.
Prèvost, F., 1994. Comportement de particules solides polydispersees dans un jet d'air turbulent. Thesis, INP, Toulouse, France.
Prèvost, F., Boree, H., Nuglish, J., Charnay, G., 1996. Measurements of fluid/particle correlated motion in the far field of an axisymmetric jet. Int. J. Multiphase Flow 22 (4), 685–701.
Qiu, H.H., Sommerfeld, M., 1992. A reliable method for determining the measurement volume size and particle mass fluxes using phase-Doppler anemometry. Exp. Fluids 13, 393–404.
Saffman, P.G., 1965. The lift on a small sphere in a slow shear flow. J. Fluid Mech. 22, 385–400.
Saffman, M., 1987. Automatic calibration of LDA measurement volume size. Appl. Opt. 26 (13), 2592–2597.
Saffman, M., Buchhave, P., Tanger, H., 1984. Simultaneous measurement of size, concentration and velocity of spherical particles by a laser Doppler method. In: Proceedings of the Second International Symposium on Applications of Laser Anemometry to Fluid Mechanics, Lisbon, Portugal, July 2–4.
Sommerfeld, M., 1997. Analysis of isothermal and evaporating turbulent sprays by Phase-Doppler anemometry and numerical calculations. In: Second International Symposium on Turbulence, Heat and Mass Transfer, pp. 55–68.
Sommerfeld, M., Qiu, H.H., 1995. Particle concentration measurements by phase-Doppler anemometry in complex dispersed two phase flows. Exp. Fluids 18, 187–198.
Van Den Moortel, T., Santini, R., Tadrist, L., Pantaloni, J., 1997. Experimental study of the particle flow in a circulating fluidized bed using a phase Doppler particle analyser: a new post-processing data algorithm. Int. J. Multiphase Flow 23, 1189–1209.
Zhu, J.Y., Rudoff, R.C., Bachalo, E.J., Bachalo, W.D. 1993. Number density and mass flux measurements using the phase Doppler particle analyzer in reacting and non-reacting swirling flows. In: Proceedings of the 31st Aerospace Sciences Meeting & Exhibit, Reno, USA, January 11–14.